Bulg. J. Phys. **33** (2006) 25–38

Interferometric Control of the Absorbing Liquids

Hr. Stoyanov

University of Sofia, Faculty of Physics, Dept. Quantum Electronics,
5 James Bourchier Blvd, BG-1164 Sofia, Bulgaria

Received *20 July 2006*

Abstract. The attenuated total internal reflection (ATIR) is an area of constant interest. The reason for that is the great variety of useful applications based on this phenomenon. In this paper we describe a simple interferometric phasemeter which can be used to control the presence of absorption in water solutions. In the process of the attenuation of the total internal reflection in a three layer system the phase shift between both main polarization components of the reflected field is strongly dependent on the complex value of the index of refraction of the second media. This method is based on the interferometric restoration of both p- and s-components of the resultant field. The resulting interferometrical signal is modeled theoretically and studied experimentally.

PACS number: 42.25.Gy, 07.60.Ly, 42.25.Ja, 78.68.+m, 42.25.Bs

1 Introduction

The great variety of useful applications is the reason why the total internal reflection (TIR) [1] is an area of constant interest. The attenuated TIR (ATIR) can be used for creating fixed or variable phase retarders [2,3,6], variable filters [4], modulators, in refractometry, for biotissue study [5], absorbing liquids [14], for investigation of surface relief [15], *etc*. Many experimental works in this field, mainly in the region of the longer wavelengths (infrared [1] and microwaves [11]) have been carried out so far. The small values of the wavelengths in visible make the investigations of the amplitude and phase changes accompanying the processes of attenuating TIR difficult. On the other hand, the interferometers as precise measuring tools bring up the research at higher level of accuracy. Interferometry is a well established and highly developed method covering very large area of applications (see *e.g.* [19,20]).

Based on a very simple method for restoration of both p- and s-components of the ATIR field and the phase shift between them, the present paper describes an interferometric application for monitoring of the presence of absorption in water

solutions. The phase shifts caused by the imaginary part of the complex value of the index of refraction of the second medium filling the constant thickness gap, even in the case of weak absorption, can be studied in this way. The theoretical prediction of the polarization dependence of the fringe topography was confirmed by the measurements.

2 The Optical Setup

In the process of TIR [12] both fields, the incident and the reflected, can be regarded as compositions of two independent fields: the p- and s-components. The reflection of a plane monochromatic wave falling on the plane boundary between two media, the first of which is denser and the second one is rarer, is highly dependant on the optical properties of a medium placed in the proximity of the plane boundary. It leads to attenuating of the TIR, which means that not only phase shifts but also amplitude losses of both field components will be observed. If the space in the so formed gap is filled with medium with complex index of refraction, the output complex amplitudes of the p- and s-component will be functions of the optical parameters of the intermediate medium. The process of reflection is highly polarization dependant and each component of the light carries information of all parameters of the system. In a system with time independent parameters any changes in index of refraction of the medium in the gap will influence the reflected field. To study the phase shifts and the amplitude changes accompanying this phenomenon we use a simple shearing interferometer which allows us to extract from the reflected wave both p- and s-components and to let them interfere in a proper way. We suppose that minimum distortions will be introduced. One possible solution of this problem is shown in Figure 1.

The optical system used in the experiment (Figure 1) consists of a laser source L of linearly polarized light, which is expanded and collimated by the collimator K. The plane wave so obtained propagates through the TIR prism PR and the shearing interferometer consisting of a polarization beamsplitter R and a linear polarizer Pol. The interferometric fringes are detected by an image array sensor Det and analysed by a PC-AT compatible computer. All elements are mounted on a vibration-isolated optical table. The elements form a common path type polarization shearing interferometer which details and theory are described in [34].

Let the incident wave be linearly polarized with azimuth ε and components $E_x \equiv E_p = |\mathbf{E}| \cos\varepsilon$ and $E_y \equiv E_s = |\mathbf{E}| \sin\varepsilon$ for the p- and s-polarization, respectively, and the ATIR complex amplitude reflection coefficients be

$$\hat{r}_p = \rho_p \exp(i\delta_p) \tag{1}$$

$$\hat{r}_s = \rho_s \exp(i\delta_s)\,. \tag{2}$$

The detector (Figure 1) is a linear photodiode array oriented along the x axis.

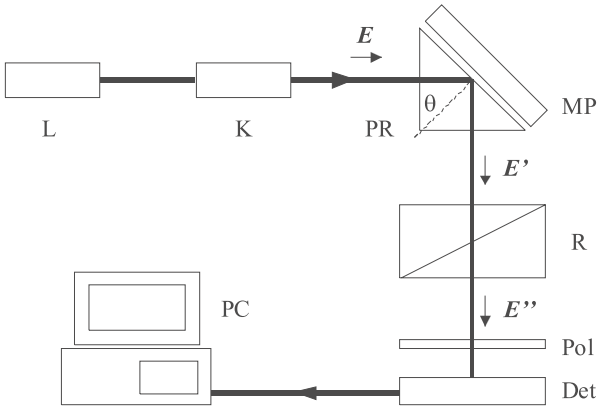

Figure 1. Sketch of the equipment: L – laser source; K – collimator; PR – TIR glass prism; MP – metal plate; R – Rochon prism; Pol – linear polarizer; Det – photodiode array detector; PC – personal computer with a framegraber.

The measured interference fringe intensity distribution is

$$I(x) = I_0 \cos^2(\varepsilon) \cos^2(\gamma) \left\{ \rho_p^2 + \rho_s^2 \tan^2(\varepsilon) \tan^2(\gamma) + 2\rho_p \rho_s \tan(\varepsilon) \tan(\gamma) \cos\left[\Phi(x, \Delta)\right] \right\}, \quad (3)$$

where the phase term has the form

$$\Phi(x, \Delta) = (\mathbf{k_p} - \mathbf{k_s}) \cdot \mathbf{r} + \frac{2\pi}{\lambda} d(x) \left[n_o - \frac{n_e(\beta)}{\cos(\beta)} \right] + \Delta,$$

and $\Delta = \delta_p - \delta_s$, β is the angle deviation between the ordinary and the extraordinary rays at the exit of the Rochon prism, γ is the azimuth of the polarizer (measured from the plane of incidence), $d(x)$ is the current thickness of the second right angle prism of the Rochon prism, $\mathbf{r}$ is the radius vector of the point of measurement. In our case it lays in $0xz$ plane, $\mathbf{k_p}$, $\mathbf{k_s}$ are the wave vectors of the ordinary and extraordinary waves, which are corresponding to the p- and s-components of the ATIR field, respectively.

The coordinate system is oriented so that the z axis is along the direction of propagation of the laser beam and the x axis lies in the plane of incidence. As a polarization beam splitter is used a quartz Rochon prism which compared with the Wollaston prism gives smaller value of the angular shear β. It also preserves the direction of propagation of the incident wave (for the ordinary wave, which coincides with the p-component of the TIR field). This proved to be an advantage in the process of aligning of the optical system.

The first two terms in Eq. (3) form the carrier frequency of the interferometric signal. For a plane wave this signal represents a family of straight parallel

fringes. The third term ($\Delta = \delta_p - \delta_s$) in (3), which is a function of additional physical and geometric parameters leads to a distortion of the basic set of fringes, provided the azimuth angles ε and γ are kept constant. It is obvious that ρ_p, ρ_s and Δ are functions of the gap thickness h, of the angle of incidence, and of the optical properties of all media the wave is passing through. In our case the assumption for low absorption dependence of ρ_p, ρ_s is not well possible. All these considerations supported with finer fringe contrast measurements show us that the process of ATIR reflection leads to strong variations in the topography of the fringes.

3 The Experimental Setup and the Initial Calibration

The source of linearly polarized coherent light in Figure 1 is a HeNe laser (Melles Griot, 3 mW) working in TEM_{00} mode. The beam is expanded and collimated up to approximately 50 mm dia by a well corrected collimator (Jodon , model BET-50 with 10 μm pin hole spatial filter). Only a small central area of the aperture was used (approximately 2×15 mm) to reduce the influence of the Gaussian profile. The plane wave at $\lambda = 632.8$ nm propagates through the TIR prism PR which was made of optical glass with $N_3 = 1.56687$. The polarization interferometer consists of a crystal quartz Rochon prism and sheet linear polarizer. The Rochon prism gives angular shear β of about 1.77×10^{-4} rad so that only four fringes (the basic 'carrier' interference pattern) are covering the full aperture of the sensor. The photodiode array has 512 elements each 28×16 μm and the pitch is 28 μm (Matsushita, model MN-512K). The azimuth of the input linearly polarized wave was adjusted at $+45^\circ$ according to x-axes with a $\lambda/2$-plate (Carl Zeiss, Jena). The analog-to-digital converter of the slot card framegraber provides 8 bit quantization of the video signal, scanning time can be programmed from 4 ms to 16 s. Special attention has been paid to the measurement of the gap width h. This was carried out by following the white light Fizeau fringes displacement localized in the gap by means of measuring microscope (not shown in Figure 1) with long working distance lens (about 122 mm). The h-value adjustment was realized with tree point micro-screw stage and piezotransducer on it charring the sample.

The starting point of every measurement was an initial calibration procedure. In the initial state, when the gap is empty, a plane silicon sample was manipulated by the three micro-screws and the transducer to be adjusted up to almost parallel position against the glass plane of the TIR prism. Then the area of the sample was adjusted to get in contact with the plane of the prism. From this initial situation the sample was translated step by step in z direction away from the glass surface. The dark brown-yellow fringe ($\lambda = 419$ nm approximately) was registered by the microscope. Only one fringe from the basic (carrier) pattern has to be affected by ATIR (Figure 2). The rest of the carrier pattern was used for comparison. Additional correction of the values of h due to the influence of

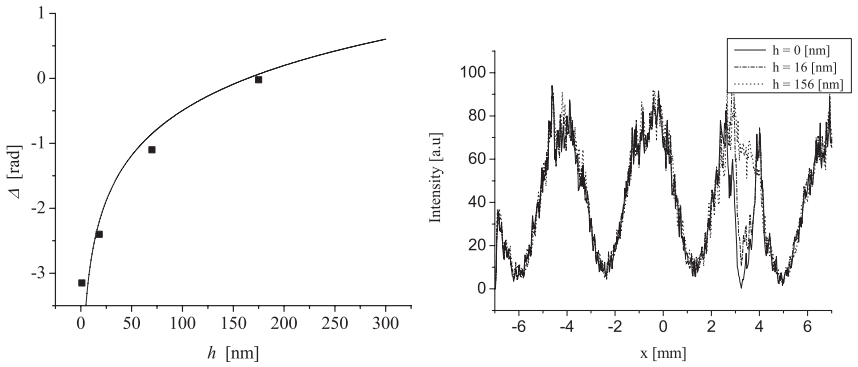

(a) (b)

Figure 2. (a) The phase shift $\Delta = \delta_p - \delta_s$ as a function of the gap thickness h: comparison between the theoretic curve (solid line) and the experimental results. (b) Photometric sections of the fringe intensity distribution in the detector aperture for three values of the gap thickness h. In both figures the attenuator was a bulk polished plate of silicon mono-crystal, N-type, cut at $(1, 0, 0)$ ($N_1 = 3.85 - i0.02$ at $\lambda = 632.8$ nm [10]).

the prism observation was carried out. The range of variation of the values of h was chosen to be less than 300 nm (an interval approximately equal to $\lambda/2$). The reason for this was to avoid the ambiguity connected with the change of the phase sign.

A typical phase shift dependence of the gap width h (for a gap space filled with air) is shown in Figure 2(a) in comparison with the theoretical model. In Figure 2(b) are shown the three typical photometric sections of the interferometric field carried out with the linear array detector. In this case the attenuator was a bulk polished plate of silicon mono-crystal, N-type, cut at $(1, 0, 0)$ ($N_1 = 3.85 - i0.02$ at $\lambda = 632.8$ nm [10]). The gap width variations are in the vicinity of the fourth fringe. There is a good agreement between the predicted and the measured values near the contact. With rising h progressive discrepancy between theory and experiment is observed.

4 Discussion of the Fringe Topography

The three layer system consisting of a dielectric first medium, an absorbing thin film and an almost perfectly conducting high impedance attenuator offers a great dynamics in the topography of the output interferometrical signal. To explain this phenomenon we express it in terms of the Stokes parameters of the ATIR field. All of them are highly nonlinear function functions of the gap width h, of the optical properties of all media and of the boundary geometry (still supposed to be plane). Let's have an optical setup similar to that described in Section 2. As we deal with monochromatic light, the p- and s-components directly define

the polarization state of the wave. As the polarization state of the light is fully described by the Stokes parameters, we will rewrite the low of two-wave interference (3) in terms of these parameters.

The Stokes vector $\mathbf{S}\left(S_0, S_1, S_2, S_3\right)$ of the incident field $\mathbf{E}$ is related to the Stokes vector $\mathbf{S}'\left(S_0', S_1', S_2', S_3'\right)$ of the ATIR field $\mathbf{E}'$ by [27,28]

$$\mathbf{S}' = \mathbf{M_{ATIR}} \cdot \mathbf{S}, \tag{4}$$

where $\mathbf{M_{ATIR}}$ is the Mueller matrix for ATIR. This matrix has the form [6]

$$\mathbf{M_{ATIR}} = \begin{bmatrix} m_{11} & m_{12} & 0 & 0 \\ m_{21} & m_{22} & 0 & 0 \\ 0 & 0 & m_{33} & m_{34} \\ 0 & 0 & m_{43} & m_{44} \end{bmatrix}, \tag{5}$$

and the matrix elements are

$$\begin{aligned} m_{11} = m_{22} = \frac{1}{2}\left(\hat{r}_p^* \hat{r}_p + \hat{r}_s^* \hat{r}_s\right), \quad m_{12} = m_{21} = \frac{1}{2}\left(\hat{r}_p^* \hat{r}_p - \hat{r}_s^* \hat{r}_s\right), \\ m_{33} = m_{44} = \frac{1}{2}\left(\hat{r}_p^* \hat{r}_s + \hat{r}_s^* \hat{r}_p\right), \quad m_{34} = -m_{43} = \frac{1}{2} i \left(\hat{r}_p^* \hat{r}_s - \hat{r}_s^* \hat{r}_p\right). \end{aligned} \tag{6}$$

The complex amplitude coefficients of reflection $\hat{r}_p$, $\hat{r}_s$ are functions of the angle of incidence, of the optical properties of all media, the light is passing through, the optical properties of the attenuating media and of the gap width h. In our model they are calculated from the characteristic impedance evolution [8,34,35]. So the Stokes vector $\mathbf{S}'\left(S_0', S_1', S_2', S_3'\right)$ of the exit ATIR field $\mathbf{E}'$ is also a function of all these quantities and in the same way depends on the state of polarization of the input light. The interferometric signal detected by the photodiode array can by expressed in terms of the polarization state of the ATIR wave. Denoting by $\mathbf{x}, \mathbf{y}$ the corresponding unit vectors, the complex amplitude in the exit of the polarizing beam splitter R (Figure 1) is

$$\mathbf{E}'' = E_p'' \mathbf{x} + E_s^{''} \mathbf{y} = \mathbf{E_p} + \mathbf{E_s}, \tag{7}$$

If the direction of transmission $pp\prime$ of the analyzer Pol has an azimuth γ measured from the x axes, the field in the exit pupil of the interferometer is

$$\mathbf{E_p p'} = \mathbf{E_p} \cos\gamma + \mathbf{E_s} \sin\gamma. \tag{8}$$

The intensity of the field, falling on the detector is given by the autocorrelation

$$I(\mathbf{r}) = \left\langle \mathbf{E'_{pp}} \cdot \mathbf{E^*_{pp}}' \right\rangle,$$

where the time averaging is denoted by$\langle \ldots \rangle$. Expressed in terms of the Stokes parameters of the ATIR field it gives us the measured intensity distribution

$$I(\mathbf{r}) = \frac{1}{2}\left\{S_0' + S_1' \cos 2\gamma + \left[S_2' \cos\Phi\left(x, \Delta\right) + S_3' \sin\Phi\left(x, \Delta\right)\right] \sin 2\gamma\right\}, \tag{9}$$

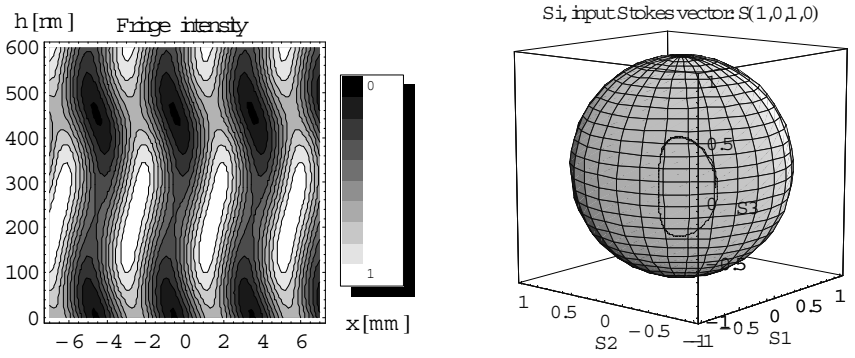

(a) (b)

Figure 3. (a) The contour plot of the theoretical fringe intensity distribution. (b) The trajectory of the Stokes vector on the Poincaré sphere. All plots as a function of the gap width h and the detector aperture coordinate x for Si attenuator and input Stokes vector $S(1,0,1,0)$ and for $n_2 = 1.33 - i0.001$.

where $\Phi\,(x,\Delta)$ is the phase function defined in (3).

This formula allows us to determine the intensity of the interferometrical signal in any point $\mathbf{r}$ as a function of the gap width h and the optical constants of all media, the light is passing through for predefined parameters of the interferometer.

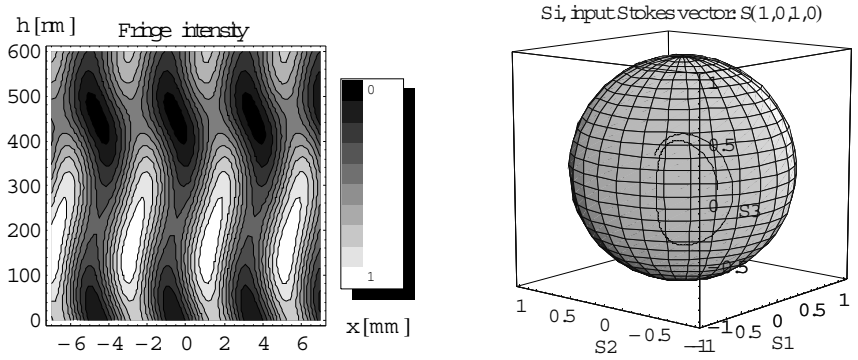

(a) (b)

Figure 4. (a) The contour plot of the theoretical fringe intensity distribution. (b) The trajectory of the Stokes vector on the Poincaré sphere. All plots as a function of the gap width h and the detector aperture coordinate x for Si attenuator and input Stokes vector $S(1,0,1,0)$ and for $n_2 = 1.33 - i0.01$.

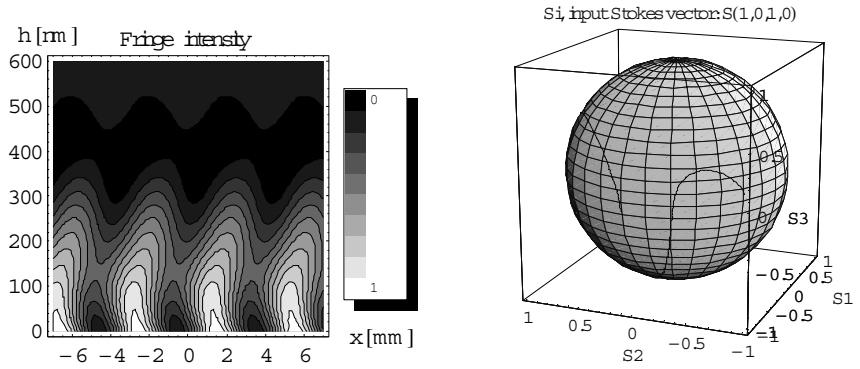

(a) (b)

Figure 5. (a) The contour plot of the theoretical fringe intensity distribution. The contour plot. (b) The trajectory of the Stokes vector on the Poincaré sphere. All plots as a function of the gap width h and the detector aperture coordinate x for Si attenuator and input Stokes vector $S(1,0,1,0)$ and for $n_2 = 1.33 - i0.1$.

A numerical model of equation (9) was realized for the case of silicon attenuator ($N_1 = 3.85 - i0.02$ for $\lambda = 0.6329$ μm [10]) and angular shear $\beta = 0.2205$ mrad. The detector aperture, placed along the x axes, is supposed to be 14 mm long, which is approximately the length of the array detector used for the measurements. The input wave is linearly polarized at $+45^\circ$ according to x-axes.

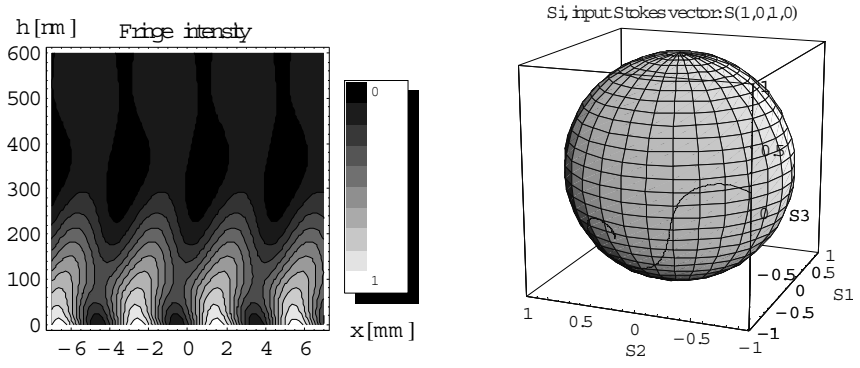

(a) (b)

Figure 6. (a) The contour plot of the theoretical fringe intensity distribution. (b) The trajectory of the Stokes vector on the Poincaré sphere. All plots as a function of the gap width h and the detector aperture coordinate x for Si attenuator and input Stokes vector $S(1,0,1,0)$ and for $n_2 = 1.33 - i0.2$.

Four examples were modeled to predict the output interferometrical signal. The gap space is supposed to be filled with water solution of weakly absorbing dye. The results are shown in Figures 3–6. They show us the process of evolution of the intensity of the output interferometrical signal (the interference fringes intensity topography) together with the evolution of the Stokes parameters of the reflected field. This evolution is shown in the form of the trajectory of the Stokes vector on the Poincaré sphere as a function of the gap thickness h. The understanding of this process is very important as the polarization interferometer combines two orthogonal components of the output field. Their mutual balance plays significant role in the process of forming of the intensity signal. When the separation h increases from zero, the output field passes through great variety of polarization states. The lower absorption leads to oscillations of the Stokes vector around the equator of the Poincaré sphere. That means the output field has a polarization state near to the liner but not exactly. The higher absorption drives the Stokes vector to the south half of the Poincaré sphere. And finely stronger absorptions make the Stokes vector to travel from the south to the north half's of the Poincaré sphere suffering rapid changes in the state of polarization. The trajectory of the Stokes vector passes near the "north pole" (right polarized elliptical wave with low eccentricity) of the Poincaré sphere and goes "down to south" to the elliptical states with still higher eccentricity, penetrates the equator (linear state) and continues in the space of the left polarized elliptical states. The inclination of the polarization ellipses during this process is varying as well.

5 Experimental Results

The object of our experiment was a water solution of malachite green day in concentrations about 10^{-2}–10^{-4} M/l. Assuming a heterogenic system of solvent host and spherical dye inclusions, the Maxwell–Garnett mixing model [36] was applied to make an estimation of the effective dielectric constant of the mixture. Two samples were studied: the first with index of refraction approximately $n_2 = 1.342 - i0.0018$ and a second one with $n_2 = 1.356 - i0.21$ at $\lambda = 632.8$ nm. The attenuating medium was a plane sample of optically polished silicon mono-crystal. The fringe intensity distribution along the detector aperture for gap width $h = 120$ nm is shown in Figure 7 and for $h = 320$ nm in Figure 8, respectively. The intensity curves are photometric slices of the intensity topography by the array detector. There is some agreement between the experimental data and the theoretical prediction. The main sources of some discrepancy are the limited precision of the visual two-beam interferometrical method, used for the gap width measurements, and the limited precision of determination of the mixture refractive index.

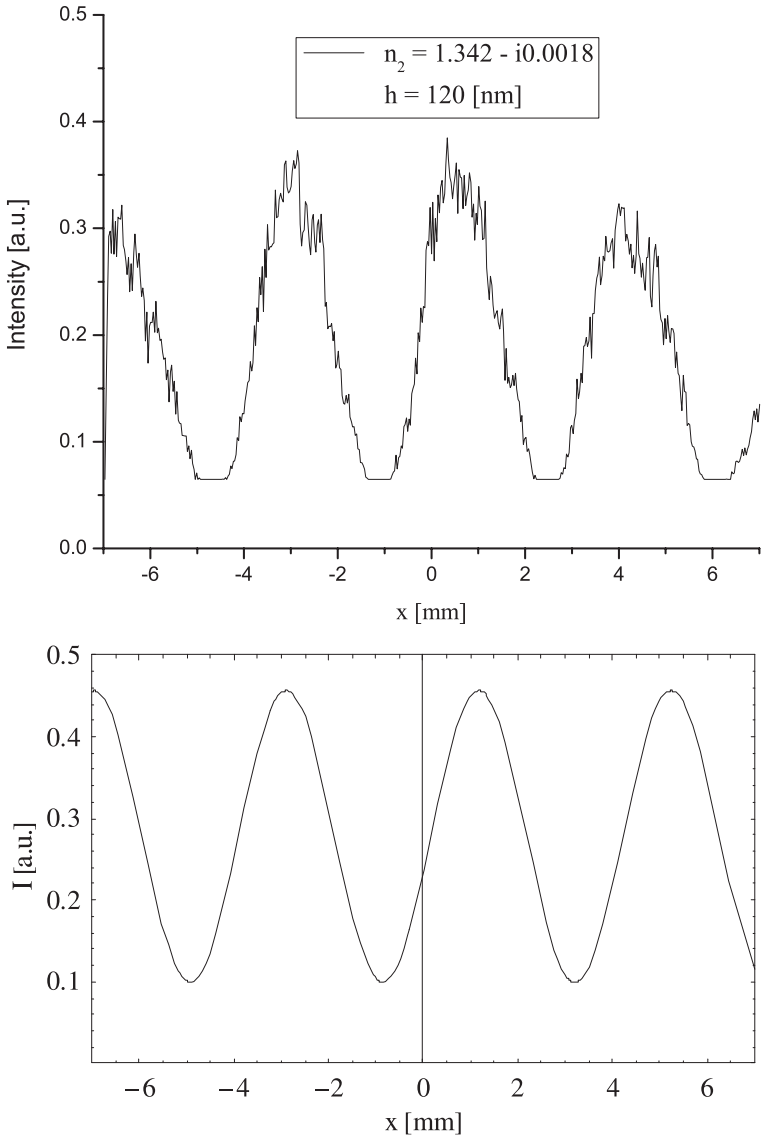

(a)

Figure 7. The experimental interference fringes intensity distribution along the array detector aperture for and gap width $h = 120$ nm compared with the theoretical prediction (a) for $n_2 = 1.342 - i0.0018$ and (b) for $n_2 = 1.356 - i0.21$.

6 Conclusion

The method described here offers an instrument for ATIR investigation of absorbing liquid medium. The experiments gave results in a quite good agreement

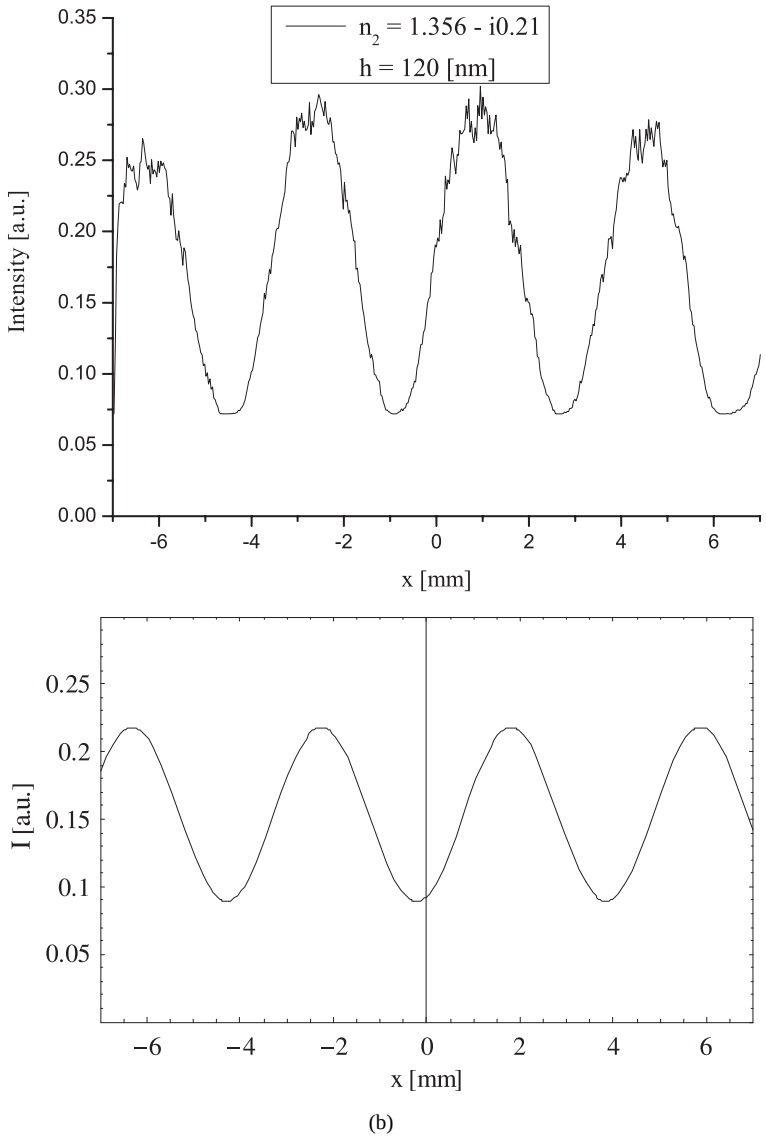

Figure 7. The experimental interference fringes intensity distribution along the array detector aperture for and gap width $h = 120$ nm compared with the theoretical prediction (a) for $n_2 = 1.342 - i0.0018$ and (b) for $n_2 = 1.356 - i0.21$.

with the theory. This method can be also applied in the case of weakly absorbing gases. An additional analysis of fringe contrast will improve the accuracy of the method of phase shift determination. The method can be used not only in

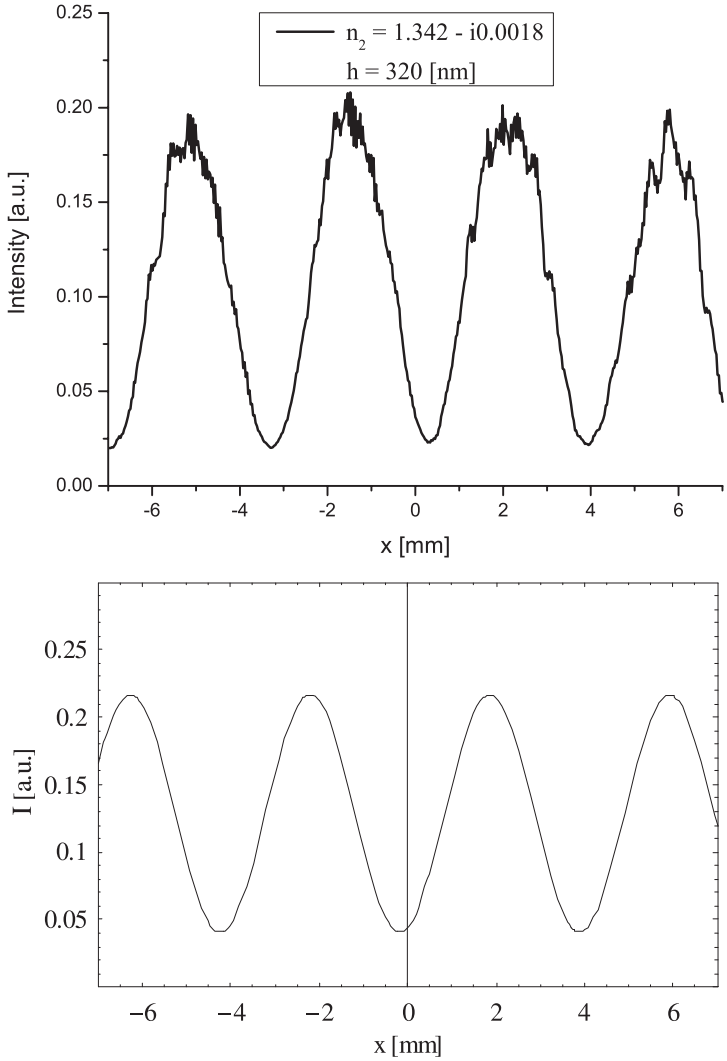

(a)

Figure 8. The experimental interference fringes intensity distribution along the array detector aperture for and gap width $h = 320$ nm compared with the theoretical prediction (a) for $n_2 = 1.342 - i0.0018$ and (b) for $n_2 = 1.356 - i0.21$.

the research, but in other applications connected with the sensor techniques like contamination monitoring, refractometry of absorbing media, *etc.*

The here described example is a good demonstration of the significance of the evolution of the polarization state of the ATIR wave, caused by variations of

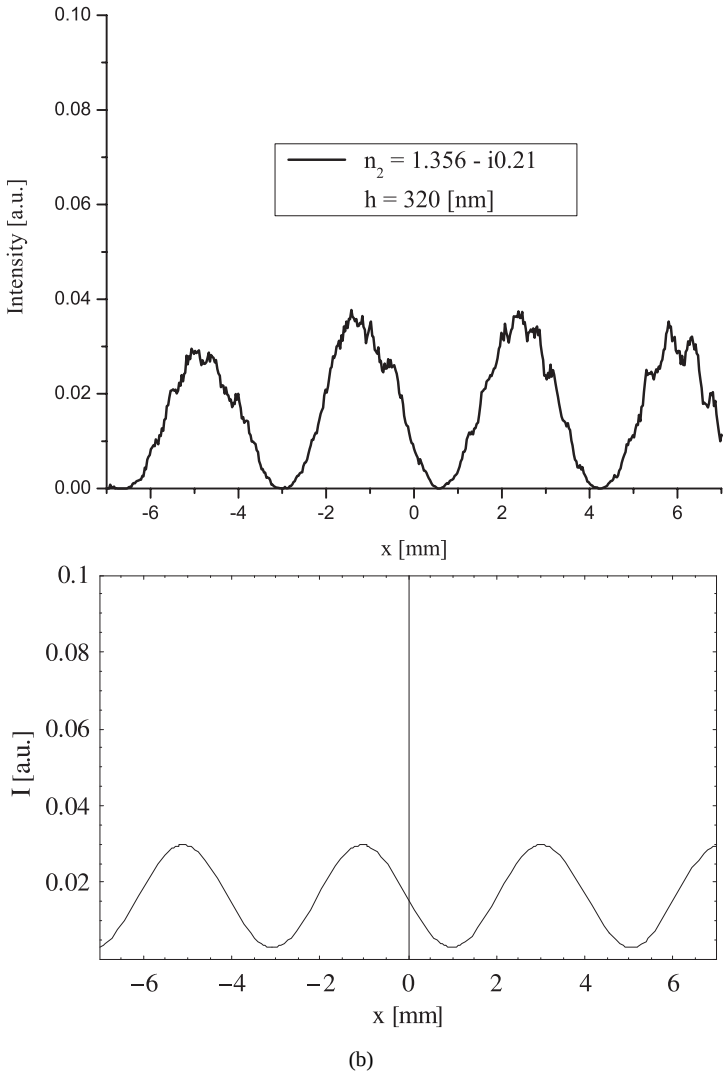

(b)

Figure 8. The experimental interference fringes intensity distribution along the array detector aperture for and gap width $h = 320$ nm compared with the theoretical prediction (a) for $n_2 = 1.342 - i0.0018$ and (b) for $n_2 = 1.356 - i0.21$.

the value of the index of refraction of medium in the gap as well as the optical properties of all media participating in the process of ATIR.

The aforementioned results will also be possibly of practical interest in the development of new methods for absorption measurements.

Acknowledgments

This work is supported by the National Fund of Scientific Research of Bulgaria, grant No. VUF 02/05.

References

[1] E.E. Hall (1902) *Phys. Rev.* **15** 73; (1905) *Phys. Rev.* **21** 346.
[2] A.M. Kan'an, R.M.A. Azzam (1994) *Opt. Engineering* **33** 2029.
[3] E. Cojocaru (1994) *Appl. Optics* **33** 7425.
[4] Yu. Wang (1995) *Appl. Phys. Lett.* **67** 2759.
[5] H. Li, Sh. Xie (1996) *Appl. Optics* **35** 1793.
[6] E. Spiller (1984) *Appl. Optics* **23** 3544.
[7] H. Heinzelman, D.W. Pohl (1994) *Appl. Phys. A* **59** 89.
[8] W. Culshow (1972) *Appl. Optics* **11** 2639.
[9] Z. Knittl (1976) *Optics of thin films*, J. Willey, New York.
[10] R.M.A. Azzam (1985) *Appl. Optics* **24** 513.
[11] W. Culshow, D.S. Jones (1953) *Proc. Phys. Soc.* **B66** 859.
[12] M. Born, E. Wolf (1959) *Principals of Optics*, Pergamon Press, London.
[13] W.A. Shurcliff (1966) *Polarized Light*, Harvard UP.
[14] S. Sainov, O. Tonchev (1989) *Optics and Lasers in Eng.* **10** 17.
[15] S. Sainov, O. Tonchev (1991) *Optics and Lasers in Eng.* **15** 267.
[19] W.H. Steel (1967) *Interferometry*, Cambridge UP.
[20] D. Malacara (1978) *Optical Shop Testing*, McGraw-Hill, New York.
[21] J.M. Bennett, H.E. Bennett (1978) in *Handbook of Optics*, McGraw-Hill.
[22] H.Y. Stoyanov (2000) *Optics and laser technology* **32** 147.
[23] A.R. Thompson, J.M. Morgan, G.W. Swenson (1986) *Interferometry and synthesis in radio astronomy*, McGraw-Hill, New York.
[24] V.Yu. Beckman (1999) *Technical Physics* **44** 1103.
[25] F. Schafers (1999) *Appl. Optics* **38** 4074.
[26] E. Collett (1968) *Am. J. Phys.* **36** 713.
[27] A.S. Marathay (1965) *J. Opt. Soc. Am*. **55** 969.
[28] A.S. Marathay (1966) *J. Opt. Soc. Am*. **56** 619.
[29] Yu. Svirco, N. Zheludev (1998) *Polarization of Light in Nonlinear Optics* J. Willey, New York.
[30] Ch. Brausseau (1995) *Opt. Letters* **20** 1221.
[31] J.M. Bueno (2000) *J. Opt. A: Pure Appl. Opt.* **2** 216.
[32] Landolt-Börnstein, Band II, 8 Teil, (1967) *Optishe Konstanten*, Heidelberg.
[33] B.E.A. Saleh, M.C. Teih (1991) *Fundamentals of Photonics*, J. Wiley, New York.
[34] H. Y. Stoyanov (2000) *Journal of Optics and Laser Technology* **32** 147.
[35] H.Y. Stoyanov (2003) *Journal of Optics and Laser Technology* **35** 409.
[36] C. Erlick (2006) *Journal of the Atmospheric Sciences* **63** 754.